Materials Chemistry and Physics 311 (2024) 128510

Contents lists available at ScienceDirect

Materials Chemistry and Physics

journal homepage: www.elsevier.com/locate/matchemphys

Electrochemical valorization of HMF using Ni/Graphite electrodes

David Carvajal, Ramón Arcas, Laxman Gouda, Francisco Fabregat-Santiago **, Elena Mas-Marzá *

Institute of Advanced Materials (INAM), Universitat Jaume I, 12006, Castelló, Spain

HIGHLIGHTS

- Biomass valorization accomplished using cost-effective NiO–OH electrodes.
- Meticulous optimization of the reaction conditions to prevent biomass degradation.
- Impedance analysis allow to detect adsorption of intermediate on the electrode.

GRAPHICAL ABSTRACT

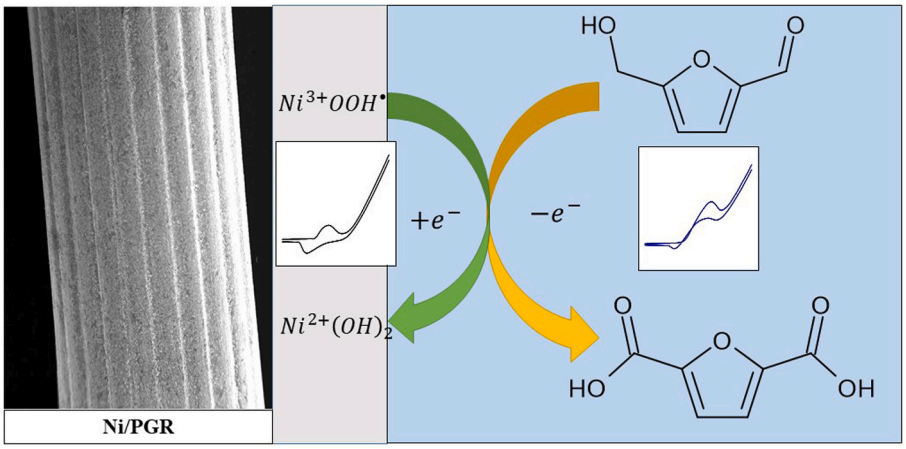

ARTICLE INFO

Keywords:
Biomass
HMF
FDCA
Electrochemistry
Impedance spectroscopy
Ni-based electrodes

ABSTRACT

The electrooxidation of 5-hydroxymethylfurfural (HMF) into 2,5- furandicarboxilic acid (FDCA) has been successfully accomplished using cost-effective NiO–OH electrodes, prepared through Ni electrodeposition on pencil graphite rods (Ni/PGR). Through meticulous optimization of the reaction conditions to prevent HMF degradation, we achieved almost complete conversion of HMF into FDC, in less than 2 h, with a remarkable 88 % Faraday efficiency. Electrochemical analyses have confirmed that our $Ni(OH)_2/NiOOH^{\bullet}$ catalyst requires a 0.16 V lower overpotential for HMF oxidation compared to water oxidation. Fitting the Impedance Spectroscopy (IS) spectra of the system have allowed us to elucidate, the details of the electrical response associated to HMF oxidation. These studies have revealed that following HMF activation, the surface of the Ni/PGR electrode remains coated with the reaction intermediates, thus triggering the complete oxidation to FDCA.

* Corresponding author.
** Corresponding author.
E-mail addresses: fabresan@uji.es (F. Fabregat-Santiago), emas@uji.es (E. Mas-Marzá).

https://doi.org/10.1016/j.matchemphys.2023.128510
Received 3 July 2023; Received in revised form 22 September 2023; Accepted 30 September 2023
Available online 9 October 2023

1. Introduction

The quest for cost-effective and environmentally sustainable synthetic methods, as alternatives to conventional approaches reliant on fossil fuels, has become imperative for industry. This is not only crucial for mitigating climate change but also for averting the inevitable depletion of these finite energy resources [1]. Within this context, electrocatalysis has emerged as a suitable synthetic methodology that avoids the use of harsh reaction conditions and fossil fuels [2]. Besides, in electrochemical approaches, the application of an electric potential difference allows performing chemical transformations that in normal atmospheric conditions would not take place [3].

The main chemical procedures studied in electrochemistry are water splitting and CO_2 reduction [4]. In both cases, the oxygen evolution reaction (OER) takes place at the anode, providing the electrons and protons needed in the cathode for the generation of H_2 or the conversion of CO_2 into valuable species, such as CO, CH_4, CH_3OH or C_{2+} compounds [5]. The OER produces O_2 that, despite being a very important compound, has low interest for the financial market, which limits the economic viability of the process and ultimately reduces the industrial interest in this technology [6]. Furthermore, this reaction exhibits sluggish kinetics and large overpotentials when using catalysts based on earth abundant materials, limiting the energy conversion efficiency [7]. For these two reasons, there is a growing interest to find alternative reactions to OER that not only reduce the overpotentials but also lead to the production of compounds with higher added-value and interest for the chemical industry [6,8]. In this framework, furanoic species, derived from biomass, have emerged as an attractive alternative to the oxidation of H_2O [9].

Furanoic species can be obtained from sugars in general but also from cellulose and lignocellulose contained in biomass, in other words, from hardwoods, softwoods, grasses, agricultural residues, etc. [10] This implies that the production of these compounds is renewable and they are available in large quantities. The main furanoic derivatives are furfural and 5-hydroxymethylfurfural (HMF). The latest one has currently gained popularity as an alternative biosource for the production of resins, solvents, pharmaceuticals, liquid fuel carriers and fine chemicals [11].

One of the products obtained in the oxidation of HMF is 2,5-furandicarboxylic acid (FDCA), a useful building block in the pharmaceutical and polymer industry [12,13]. Traditionally, HMF to FDCA oxidation involves noble metal-based heterogeneous catalysts supported on materials like C, TiO_2, RGO, Al_2O_3, and ZrO_2, using O_2 or high-pressure air as oxidants at temperatures above 100 °C, [13,14]. thus hindering the industrial scalability of this oxidation process [15].

The electrochemical oxidation of HMF to FDCA is a three-step process involving intermediate species (Fig. 1), including diformylfuran (DFF), 5-hydroxymethyl-2-furancarboxylic acid (HMFCA) and 5-formyl-2-furancarboxylic acid (FFCA). Typically, this process is conducted in alkaline conditions employing metal or metal oxide electrodes like NiO–OH [16–18], due to effective redox pair Ni^{2+}/Ni^{3+} or $Ni(OH)_2/Ni(OOH^{\bullet})$generated by the applied potential in basic solutions. The first example of the electrooxidation of HMF with NiO–OH was reported by Grabowski et al. showing a 71 % yield of FDCA at pH 14 [19]. Subsequent studies have demonstrated the oxidation of HMF reaching yields around 90–98 % of FDCA, using Ni Foam electrodes modified with Fe or Se [4,20,21]. Mechanistic studies indicate that HMF oxidation begins with the formation of Ni^{3+} or Ni(OOH•) from Ni^{2+} or $Ni(OH)_2$ on the electrode surface. Then, through a proton-coupled electron transfer (PCET) mechanism, HMF is oxidized, releasing an electron and a proton (e^-/H^+) and regenerating $Ni^{2+/}Ni(OH)_2$ on the electrode surfac [22].

In the electrochemical oxidation of HMF in alkaline conditions, one of the competing reactions involves the spontaneous degradation of HMF, leading to the formation of formate, levulinic acid, or insoluble humins [23]. Consequently, it is imperative to establish optimal reaction conditions (e.g., pH, electroactive area, etc.) that favor FDCA production over this competing decomposition [24–26]. In our recent study, we utilized planar NiO–OH electrodes, fabricated by electrodeposition of Ni on FTO, for the oxidation of low-concentration HMF solutions (5 mM), which resulted in HMF degradation [25]. To boost FDCA production and prevent HMF degradation, we propose enhancing the active area of our NiO–OH electrodes while reducing the pH of the reaction medium. Recently we have demonstrated that the electrodeposition of Ni on pencil graphite rods allows to obtained Ni-based electrodes (Ni/PGR) with much higher surface area than our earlier planar electrodes [26]. These Ni/PGR electrodes exhibit increased current densities for HMF oxidation compared to our earlier planar electrodes. This improvement can be attributed to the higher porosity of the Ni/PGR electrodes, resulting in an expanded active surface area.

Using these Ni/PGR electrodes, we achieved a 96 % HMF conversion rate, resulting in a 91 % FDCA yield and an 88 % Faraday efficiency, while yielding only 5 % of formate, at pH 13.6 (0.5 M LiOH) in 6 h. Optimization of our system allowed us to reduce the reaction time to just 100 min while maintaining similar levels of conversion, yield, and

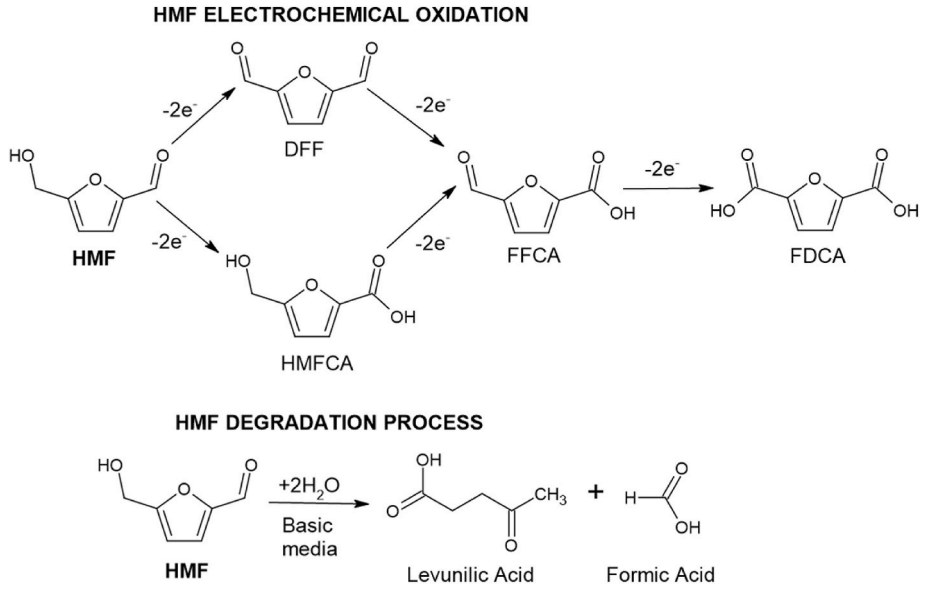

Fig. 1. HMF oxidation and degradation process in basic media.

Faraday efficiency. To gain a deeper insight into the electrochemical response of these nickel-functionalized carbon electrodes, we conducted Impedance Spectroscopy (IS) analysis using a transmission line equivalent circuit. This analysis revealed two oxidation processes, namely, Ni^{2+} to Ni^{3+} and HMF oxidation, aligning with our earlier findings from cyclic voltammetry [25]. Additionally, IS verified the adsorption of HMF and intermediary oxidation species on the electrode's surface, aligning with previous in operando measurements [27]. This underscores IS as an alternative method for detecting the adsorption of intermediate species on electrode surfaces.

2. Experimental section

Chemicals. All reagents were used from commercial suppliers without further purification. Graphite rod (Staedtler, Mars Carbon 200, 4 B 2 mm, ©STAEDTLER mars GmbH & CO, KG, made in Germany), $NiCl_2$ (99 %, Sigma-Aldrich), Na_2SO_4 (99 %, Sigma-Aldrich), LiOH (99.995 %, Sigma-Aldrich), desionized water (milliQ system, 18 MΩ*cm), LiCl (99 %, Sigma-Aldrich), HMF (5-hydroxymethyl furfural, 99 %, Sigma-Aldrich), DFCA (2,5 furandicarboxilic acid, 99 %, Sigmal-aldrich), HMFCA (5-hydroxymethyl-2-furancarboxylic acid, ≥95 %, Sigma-Aldrich), FFCA (5-formyl-2-furoic acid, 99 %, Sigma-Aldrich), DFF (2,5 furancarboxaldehyde, 99 %, Sigma-Aldrich), water HPLC grade (VWR chemicals), methanol HPLC grade (VWR chemicals).

Preparation of Ni/PGR electrodes. Ni/PGR electrodes were prepared by electrodeposition of Ni on pencil graphite rods (PGRs, 4 B hardness, 2.0 mm diameter and 13.0 mm length, ©STAEDTLER mars GmbH & CO, KG, made in Germany) following a previously reported experimental procedure [26]. Before the Ni electrodeposition, the polymeric coating of the PGRs was removed by flame treatment. This treatment consisted in burning 10 × 1 min times de PGR, leading to a porous structure of carbon. The electrodeposition of Ni on PGR was performed by cyclic voltammetry, doing 25 cycles at 50 mV/s from 0 to −1.3 V (*vs* Ag/AgCl), in a 10 mL solution of 100 mM of Na_2SO_4 and 20 mM of $NiCl_2$ in one-compartment cell, using the PGR as working electrode, a Pt wire as counter electrode and Ag/AgCl (3 M KCl) as a reference electrode. Prior to the electrochemical measurements for HMF oxidation, the Ni/PGR was activated by cyclic voltammetry, applying 25 cycles at a scan rate of 50 mV/s from 0 to 1 V (*vs* Ag/AgCl), in 10 mL of 1 M LiOH solution with magnetic stirring.

Electrochemical measurements. Cyclic voltammetries, Chronoamperometries and Impedance Spectroscopy (IS) experiments were performed with a three electrodes configuration, using both a Metrohm Autolab (PGSTAT204) and Gamry (Reference 3000^{tm}) potentiostat/galvanostat indistinctly. A Pt wire and Ag/AgCl electrode were used as counter and reference electrodes, respectively. All the potentials values were converted to RHE scale using the equation

$$V(RHE) = V(Ag/AgCl) + 0.197V + 0.0591 * pH \quad (1)$$

For all the measurements the Ni/PGR electrodes were immersed 10 mm in the electrolyte providing a geometric area of 0.66 cm^2.

Cyclic voltammetry. Measurements were done in a 10 mL solution of X LiOH/Y LiCl (with X and Y the molar concentration of each species, keeping X + Y = 1 M) in one-compartment cell with magnetic stirring. Cyclic voltammetries in the absence and presence of HMF (5, 10, 20, 30 and 50 mM), were measured at a scan rate of 5 mV/s from 1.2 to 1.8 V *vs* RHE for 10 cycles.

Chronoamperometry. The HMF oxidation experiments were performed in a two-compartment cell with three electrodes by chronoamperometry at 1.5 V *vs* RHE for 6 h. Ni/PGR (length of 2 cm, area of 1.32 cm^2) was used as a working electrode. The anolyte compartment contained 10 mL of X LiOH/Y LiCl solution (X + Y = 1 M and X = 1, 0.5 and 0.25 M) with 10 mM of HMF with magnetic stirring. Aliquots of 30 μL of the solution were taken for HLPC analysis. For the increment of the active area, the same experimental procedure was performed but using in this case five Ni/PGRs as the working electrode. The five Ni/PGR were connected among them with Cu tape.

Impedance Spectroscopy Analysis (IS). The Ni/PGR electrode was used as a working electrode (10 mm immersed in the electrolyte, providing a geometric area of 0.66 cm^2) in one-compartment cell containing 10 mL of XM LiOH/YM LiCl solution (X + Y = 1 M). The measurements of IS were done in the potential range of 1.4–1.8 V vs RHE, at steps of 25 mV. The frequency used ranged from 100 kHz to 10 mHz. The concentration of HMF used was 40 mM.

HPLC Analysis. The separation and quantification of the products from the chronoamperometry experiments were performed with a HPLC Agilent 1260 infinity II quaternary system using a Column Agilent (poroshell EC-C18, 4.6 × 100 mm, 2.7 μm) and a DAD detector (UV range was used). Conditions: the eluent used was 80%–20 % water (pH = 2.4, H_2SO_4)-methanol; elution rate of 0.5 mL/min, 40 °C of column temperature, injection of 5 μL of the sample. With these conditions, the elution took 5 min for sample separation.

Calibration curves were performed for the quantification. The calibration was done considering the relation between the absorbance and the concentration of reagent and products (at 250 nm for FDCA and HMFCA, 285 nm for HMF, FFCA and DFF and 270 nm was used for comparison of the decreased HMF signal and FDCA increased signal).

For the quantification, 30 μL of the chronoamperometry experiment was diluted with 3 mL of water (HPLC grade) and injected into the HPLC equipment.

^{1}H-NMR Analysis. The quantification of formate was done by ^{1}H NMR in a spectrometer Bruker Avance III HD 400 MHz, using deuterated water as solvent. The standard used for quantification was tert-butanol (99 % Aldrich), the relation between the signals of formate and tert-butanol was 1/9.

3. Results and discussion

We synthesized the Ni electrodes on pencil graphite rods (Ni/PGR) using our previously reported electrodeposition method with a 20 mM $NiCl_2$/100 mM Na_2SO_4 aqueous solution [26]. Based on the cyclic voltammetry curves (Fig. S1), we estimated that approximately 511 ± 7 μg of nickel was deposited within 1 cm of the PGR electrode (length of the rod). SEM images (Fig. S2) and EDS analysis (Figs. S3 and S4) of the Ni/PGR electrodes confirmed successful spherical-shaped nickel electrodeposition into the PGR matrix. Previous characterization of these electrodes by XPS revealed a mixed phase of metallic and oxidized Ni. Quantifying each state showed an equal concentration of Ni^{2+} species, suggesting that electrodeposition resulted in Ni^0 species rather than Ni^{3+}. [26].

Fig. 2A depicts the electrochemical performance of the porous Ni/PGR electrodes in 1 M LiOH, from 1.2 to 1.8 *vs* RHE, with different concentrations of HMF. The selection of LiOH as the electrolyte is grounded in our prior investigations, which substantiated its efficacy in enhancing the oxidation of HMF in comparison with other alkali electrolytes [25]. In general, the cyclic voltammetry patterns closely resembled those observed in our prior investigations involving planar NiO–OH electrodes [25]. Interestingly, the current achieved at the redox peaks associated to the oxidation of Ni and HMF exhibited a tenfold increase when compared to the planar NiO–OH electrodes the planar NiO–OH electrodes. This increase can be attributed to the significantly larger electrode surface area provided by the Ni/PGR.

In the absence of HMF, the typical response for Ni electrodes in basic media was obtained, with the characteristic redox peak for the Ni^{2+}/Ni^{3+} transition, here $Ni(OH)_2/Ni(OOH^{\bullet})$, found between 1.4 and 1.5 V. The width of this peak has been recently associated with the presence of different hydrated and non-hydrated phases of Ni species [26]. At potentials higher than 1.6 V *vs* RHE, the linear increase of the current observed corresponds to the OER.

In the presence of HMF, Ni was firstly oxidized from $Ni^{2+}$to Ni^{3+}, and then Ni^{3+} oxidizes HMF leading to a second oxidation peak that overlaps with the Ni^{2+}/Ni^{3+} redox peak and increases with the concentration of

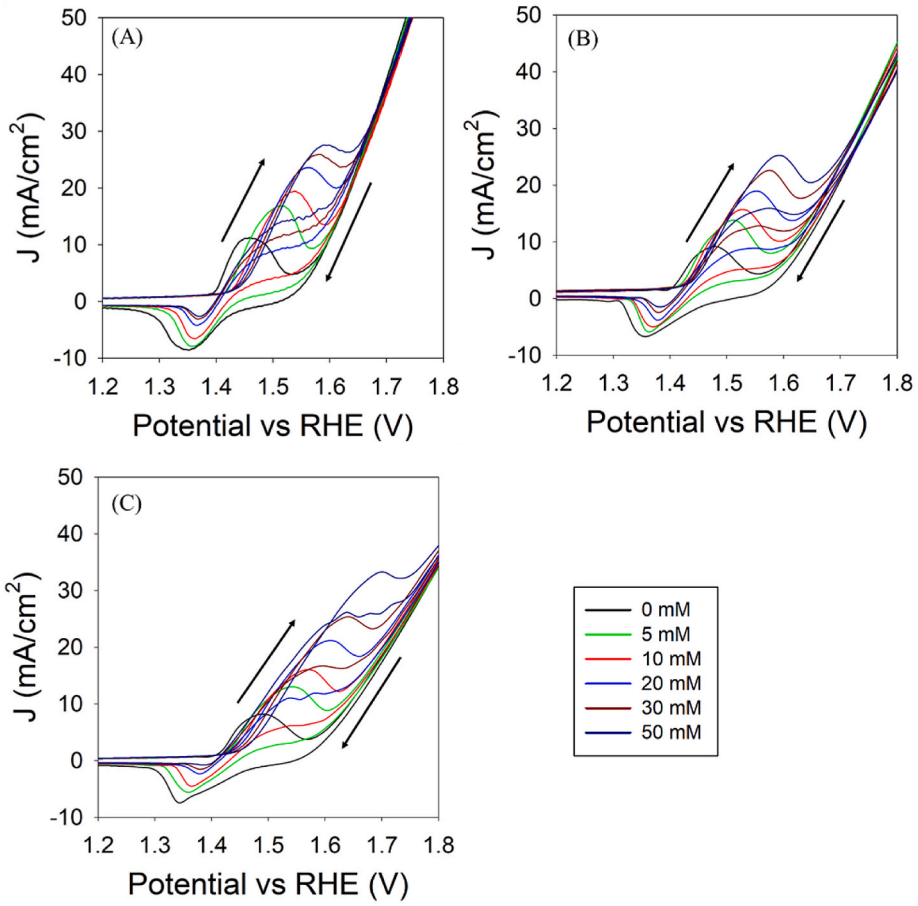

Fig. 2. Cyclic voltammetries for the oxidation of HMF (0–50 mM), using Ni/PGR as working electrode, Pt as counter electrode and Ag/AgCl as reference (RHE potential scale), in A) 1 M LiOH, B) 0.5 M LiOH/0.5 M LiCl. C) 0.25 M LiOH/0.75 M LiCl as electrolyte at 5 mV/s scan.

HMF. Furthermore, we noted a shift in the onset and oxidation peaks (both for Ni^{2+}/Ni^{3+} and HMF oxidation) toward higher potentials as the HMF concentration increased. This phenomenon can be attributed to the greater quantity of HMF adsorbed onto the electrode's surface. The adsorption of HMF partially blocks the Ni/PGR electrode surface, introducing an additional potential loss for Ni oxidation and causing the HMF oxidation reaction to shift by several tens of mVs. The substantiation of HMF adsorption and the presence of intermediate species is discussed in the context of Impedance Spectroscopy (refer to the discussion in Fig. 6).

Focusing now on the reduction direction of the CV, the reduction peak of Ni (Ni^{3+}/Ni^{2+}), at 1.3–1.4 V *vs* RHE, decreased with the amount of HMF. Moreover, at 1.5 V *vs* RHE in the presence of HMF, the current was positive, indicating that the HMF oxidation was still taking place. As Ni^{3+} is consumed during this reaction, the height of its reduction peak at 1.3–1.4 V *vs* RHE decreases while increasing the concentration of HMF. This observation aligns with recent findings that have demonstrated the formation and subsequent consumption of Ni^{3+} or NiOOH × species during the oxidation of organic compounds, as evidenced through in situ surface Raman spectroscopy [28].

Fig. 2B depicts the electrochemical response for HMF oxidation in 0.5 M LiOH/0.5 M LiCl, showing a similar behaviour than in 1 M LiOH. The currents obtained for the redox reactions were similar, thus demonstrating that the redox pair could also be activated with 0.5 M of LiOH. The main difference between Fig. 2A and B was detected in the OER region, showing that a decrease in the amount of LiOH led to a reduction in the kinetics for the formation of O_2.

Fig. 2C shows the CV in 0.25 M LiOH/0.75 M LiCl. In this case, the density of the current response showed some delay in relation to the potential when compared to prior cases (1 M and 0.5 M LiOH). Additionally, the oxidation peaks, specifically Ni^{2+}/Ni^{3+} and HMF oxidation, displayed elevated resistance and were observed in closer proximity to the onset of OER. In general, changes in the concentration of LiOH produce variations of the amount of $Ni(OH)_2$ electroactive species on the surface of the electrode and the redox potential of Ni^{2+}/Ni^{3+} [29]. We have observed that a decrease of the concentration of LiOH decreases the kinetics of HMF oxidation and HMF degradation. In our case, the best results obtained (vide infra) in terms of competition between HMF oxidation and degradation were using 0.5 M LiOH/0.5 M LiCl.

To study the electrochemical oxidation of HMF to FDCA, chronoamperometric experiments were performed at 1.5 V (*vs* RHE). The results for the oxidation of 10 mM HMF with Ni/PGR electrodes (active area of 1.32 cm^2) in 1 M LiOH, 0.5 M LiOH/0.5 M LiCl and 0.25 M LiOH/0.75 M LiCl solutions are depicted in Fig. 3 and results are shown in Table 1. The detection and quantification of HMF and FDCA were performed by HPLC (see experimental section and Figs. S5–S6 for details). Intermediates HMFCA and FFCA (Fig. S7), were detected in very low concentration in all cases (<1 %). It has been reported that the mechanism of HMF oxidation is pH dependent, due to how HMF interacts with the surface of the electrode. For pH > 13, the reaction goes through the formation of HMFCA, whereas for pH < 13, the oxidation proceeds through DFF production [10]. In our experiments, the pH was always higher than 13, and the analysis by HPLC revealed that the oxidation of HMF proceeded by the HMFCA route (see Fig. 1).

In the case of 1 M LiOH (pH = 14), a decrease in the concentration of HMF was observed, with conversions of 50 %, 80 % and 96 % after 1, 3 and 6 h of reaction, respectively (Fig. 3A). Simultaneously, an increase in the concentration of FDCA was detected during the reaction, with 42

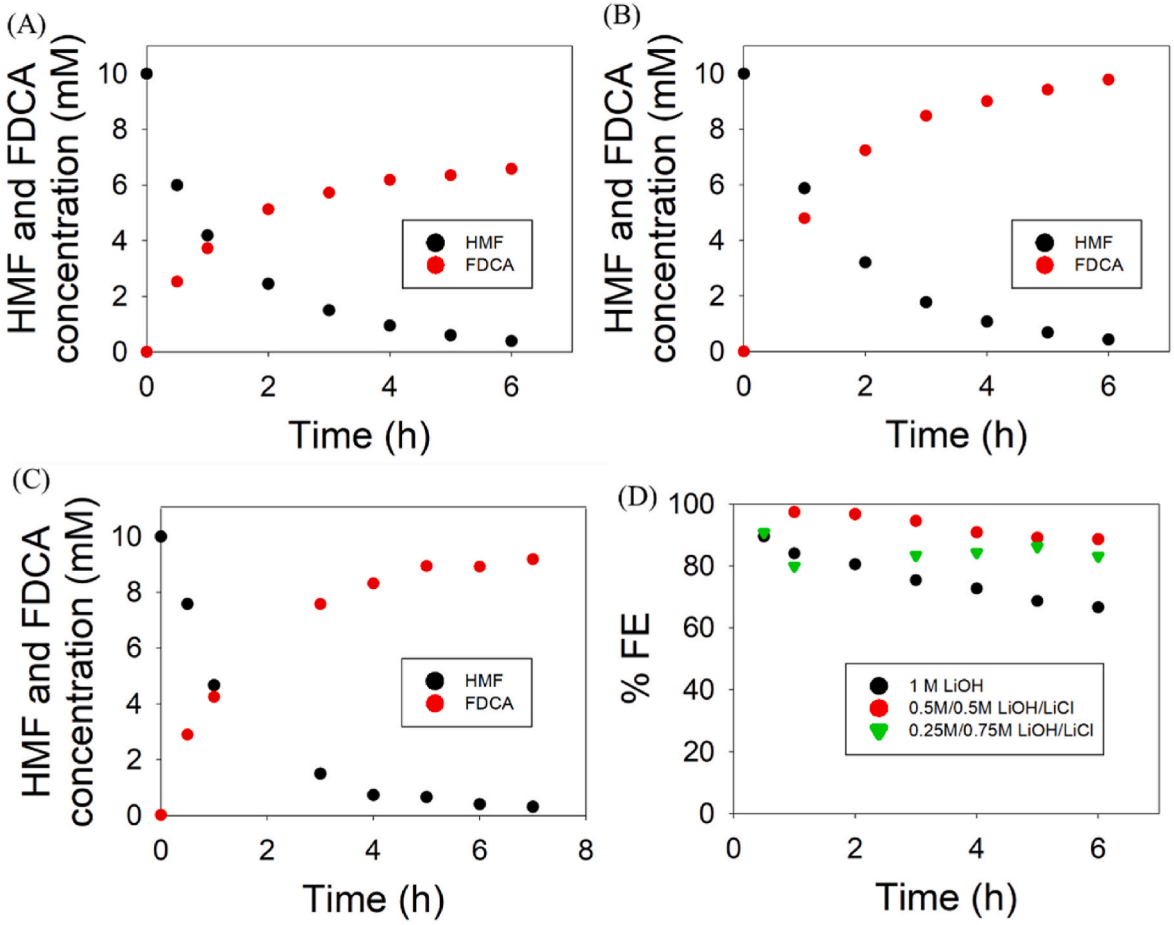

Fig. 3. HMF and FDCA concentration *vs* time, for 10 mM of initial concentration of HMF, using Ni/PGR as working electrodes at 1.5 V *vs* RHE, in A) 1 M LiOH; B) 0.5 M LiOH/0.5 M LiCl; C) 0.25 M LiOH/0.75 M LiCl. D) Evolution of the FE for the formation of FDCA *vs* time.

Table 1
HMF conversion, FDCA and formate yields, and final Faraday efficiency for the formation of FDCA during the chronoamperometries at 1.5 V *vs* RHE.

Electrolyte	HMF conversion (%)	FDCA yield (%)	Formate yield[a] (%)	FDCA FE (%)	Time (h)
1 M LiOH	96	74	16	67	6
0.5 M LiOH/0.5 M LiCl	96	91	5	88	6
0.25 M LiOH/ 0.75 M LiCl	97	82	6	84	7
0.5 M LiOH/0.5 M LiCl, using 5 Ni/PGRs	>99	94	6	88	1.67

^{1}H NMR.
[a] Detection and quantification by.

% yield at 1 h of reaction, reaching nearly 74 % yield at the end of the experiment (6 h, Table 1). These results indicate that almost 20 % of the initial HMF was converted but not electro-oxidized to FDCA. Analysis by ^{1}H NMR at the end of the experiment revealed the formation of formate (see SI, Fig. S9) as main side product due to the non-electrochemical degradation of HMF in basic media [24]. By other side, the Faraday efficiency (Fig. 3D) was higher than 80 % in the first hour of the experiment while it decreased until 67 % at the end (Fig. 3D and Table 1). This observation can be elucidated by considering the competitive nature of the OER and the oxidation of HMF at 1.5 V (*vs* RHE). As a result, when the concentration of HMF remains sufficiently high, the primary reaction occurring is the organic oxidation. Conversely, once HMF is consumed, the OER proceeds more efficiently.

When the reaction was performed in 0.5 M LiOH (pH = 13.7), the conversion of HMF was similar than in 1 M LiOH (compare Fig. 3A and B), leading to a 96 % conversion at 6 h (Table 1). Notably, the yield of FDCA increased faster, reaching 91 % at 6 h of reaction. Interestingly, only a small amount of formate (nearly 5 %) was detected by ^{1}H NMR at the end of the reaction. These findings unmistakably demonstrate that reducing the hydroxide ion (OH^{-}) concentration in the reaction medium by 50 %, shifting from pH 14 to pH 13.7, promotes the electrooxidation of HMF and decelerates the degradation process. The Faraday efficiency in this case was nearly 100 % during the first 2 h of reaction and decreased to 88 % after 6 h.

A higher reduction of the initial pH to 13.4 (0.25 M LiOH/0.75 M LiCl) did not improve the overall performance of the system. As shown in Fig. 3C, in this particular scenario, a final conversion of 97% of HMF was attained after 7 h, albeit resulting in a reduced FDCA yield of 82 %. The formation of formate kept at 6 %, and the Faraday efficiency remained still reasonable (83 %). Given that the formation of the possible intermediate species was negligible, the disparity between HMF conversion and FDCA yield in this case could be linked to the formation of humin species [23]. In this scenario, the reduced performance in the reaction might be attributed to a less efficient generation of the Ni redox pair essential for the electrochemical oxidation of HMF at a pH of 13.4, Regarding the stability of our Ni/PGR electrodes in the oxidation of HMF, measurements of the solution before and after the chronoamperometry experiment by total reflection X-ray-fluorescence technique, indicated that only 0.4 % of the electrodeposited nickel was lost in the reaction media, see Fig. S1 and Table S1 in supporting information. Besides, Fig. S10 depicts seven consecutive

chronoamperometric experiments for the oxidation of 10 mM of HMF, showing a slow variation of the initial current density, thus confirming a reasonable stability of these low-cost Ni based electrodes.

We have also analyzed the kinetics for the formation of formate in the reaction media. As can be seen in Fig. S9, a higher concentration of LiOH increased the formation of formate. Noticeably, at the beginning of the experiments, an important amount of formate was produced, indicating that while HMF concentration is still high, the degradation process is in strong competition with the HMF electrooxidation.

With the aim to increase the oxidation rate of our Ni/PGR electrodes, we increased the active area to 3.3 cm^2 by using 5 Ni/PGR electrodes at the same time, connected with a Cu tape. Fig. 4A shows the cyclic voltammetry for the oxidation of HMF using 5 Ni/PGR electrodes in 0.5 M LiOH/0.5 M LiCl. The obtained response resembled that of using a single electrode, as shown in Fig. 2B. However, when utilizing all five electrodes, the achieved current was approximately three times greater. The chronoamperometry for the oxidation of 10 mM of HMF using 5 Ni/PGR electrodes in 0.5 M LiOH/0.5 M LiCl is shown in Fig. 4B. With this aggrupation of electrodes, the reaction time was significantly reduced from 6 h to just 100 min, while still achieving comparable HMF conversion, FDCA yield, and Faraday efficiency. The conversion of HMF and the formation of FDCA *vs* time during the experiment is shown in Fig. 4C and Table 1. As can be observed, the conversion of HMF was faster, reaching a conversion higher than 80 % after 1 h and nearly quantitative conversion at 100 min (1.67 h). The yield of FDCA increased following a lineal function, reaching 94 %, with 88 % Faraday efficiency after 100 min of reaction. The amount of formate formed, due to HMF degradation, was 6 %, (determined by ^{1}H NMR). These findings collectively illustrate how the clustering of Ni/PGR electrodes facilitates a significant reduction in the experimental time required for the oxidation of HMF.

Our results align with findings from previous studies. For instance, Liu et al. achieved a 97 % FDCA yield and a Faraday efficiency of 98.6 % in 90 min using NiFe layered double hydroxide (LDH) nanosheets for HMF oxidation [4]. Barwe et al. employed nickel foam decorated with nickel boride, yielding 98.5 % FDCA in 30 min with nearly 100 % Faraday efficiency in a flow cell with a flow rate of 18 mL/min [20]. Holzhäuser et al. obtained FDCA yields exceeding 80 % using modified commercial nickel oxide [21]. Notably, these examples involved complex electrode preparation processes with multiple steps. In contrast, our easily fabricated NiPGR electrodes achieve similar results, underscoring the potential of Ni/PGR for the electrochemical oxidation of HMF and related organic compounds. Moreover, the turnover frequency (*TOF*) obtained when using 0.5 M LiOH/0.5 M LiCl were comparable with previous reports for heterogeneous Ni-based catalysis [30–32], being $TOF = 28.2 \pm 0.5\ h^{-1}$ for the single Ni/PGR electrodes and $TOF = 17 \pm 1\ h^{-1}$ for the five Ni/PGR electrodes (see experimental section, Fig. S11). Table S2 presents a comparative of the results obtained with our Ni/PGR and other Ni-based electrodes from the literature.

To gain more insight about the processes occurring in the Ni/PGR electrodes, we made a detailed Impedance Spectroscopy (IS) analysis. Fig. 5 shows the J-V curve of the Ni/PGR electrodes obtained during IS experiments in 1 M LiOH and 0.5 M LiOH/0.5 M LiCl solutions, with and without HMF. In both cases, very similar results were obtained with slightly higher current in the case of 0.5 M LiOH/0.5 M LiCl, as expected from the chronoamperometry results. Without HMF, the current is negligible in the region between 1.30 and 1.55 V (*vs* RHE). After this potential the onset of the current associated to the OER is observed. In the presence of 40 mM of HMF, the current onset appeared at 1.4 V, due to the oxidation of HMF with Ni–OOH$^\bullet$ species, and then achieved a current close to 5 mA/cm^2 at around 1.5 V *vs* RHE. At 1.55 V, the OER was activated. The decrease in the overpotential needed to start HMF reaction is then 0.15 V smaller that for OER. This value is very reliable as it has been taken from the stationary J-V curve in Fig. 5, which is not affected by capacitive effects as it happens in other techniques like linear sweep or cyclic voltammetries. It is important to note that we employed the corrected potential, denoted as V_F, which accounts for the subtraction of the potential drop caused by series resistances from the applied potential.

Impedance spectra with and without HMF in a 1 M solution of LiOH are shown in Fig. S12. Similar spectra were found when using 0.5 M LiOH/0.5 M LiCl (data not shown here for simplicity). The impedance data were fitted to the transmission line equivalent circuit shown in Fig. S13 which is based on a previous reported work [26].

Fig. 6 depicts the values obtained from IS fitting for the most relevant parameters, C_{rod} and R_{ct}, in the absence and presence of HMF (0 mM and 40 mM, respectively) for 1 M LiOH solution. Similar results were obtained when using 0.5 M LiOH/0.5 M LiCl solution (not shown). In the absence of HMF, at 1.375 V *vs* RHE, C_{rod} value has a first maximum which corresponds to the current peak found in the CV in Fig. 2A, attributed to the Ni^{2+}/Ni^{3+} redox couple transition. Associated to this peak in C_{rod}, R_{ct} reaches a local minimum. At potentials higher than 1.45 V *vs* RHE, the R_{ct} presents a continuous diminution, corresponding to the approach to the region for the OER. C_{rod}, shows a peak at 1.55 V *vs* RHE where the onset for the OER occurs (see Fig. 4), which is associated to the Ni^{3+}/Ni^{4+} redox transition previous to the water oxidation reaction [25].

In the presence of HMF, some differences are found for C_{rod} and R_{ct} in comparison with data in the absence of HMF. In this case, C_{rod} presents three peaks and R_{ct} two local minimums. In the C_{rod}, the first very small peak at ~1.375 V *vs* RHE corresponds to the Ni^{2+}/Ni^{3+} redox transition. The second peak in C_{rod} and minimum in R_{ct} appears at 1.425 V *vs* RHE and corresponds to the HMF oxidation reaction and the onset of current for solutions containing HMF in Fig. 5. After this second peak, C_{rod} decreases far below the values obtained in the absence of HMF. At the same time, R_{ct} rises to a peak around 1.5 V *vs* RHE. These data suggest that intermediate species involved in HMF oxidation, as illustrated in Fig. 1, tend to remain adsorbed on the electrode surface, partially obstructing it

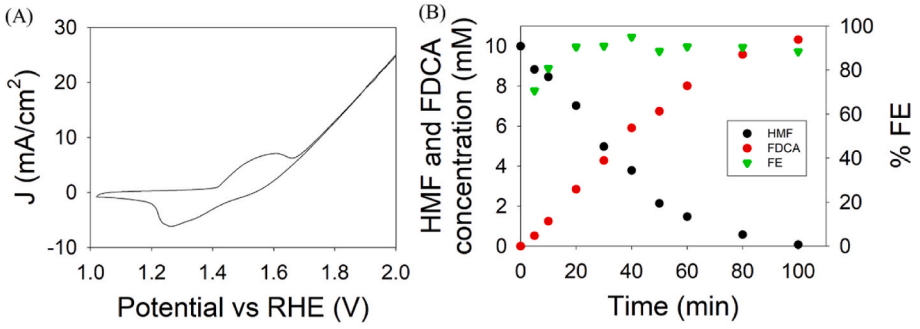

Fig. 4. A) Cyclic voltammetries using 5 Ni/PGR as working electrode, Pt as counter electrode and Ag/AgCl as reference (RHE potential scale), in 0.5 M LiOH/0.5 M LiCl, at 5 mV/s scan rate with 10 mM of HMF. B) HMF and FDCA concentration and % FE results for chronoamperometry of 10 mM initial concentration of HMF with 5 Ni/PGR as working electrode with 0.5 M LiOH/0.5 M LiCl.

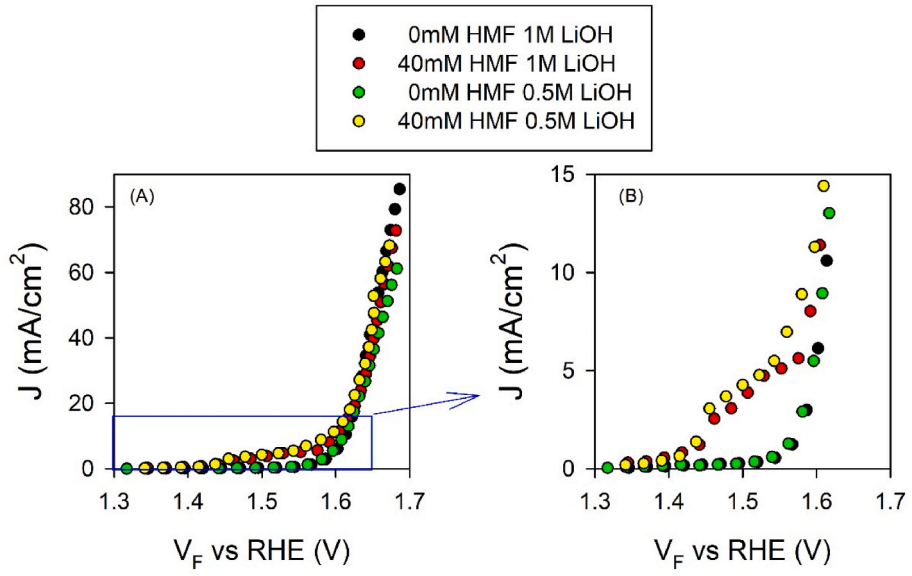

Fig. 5. J-V curves after series resistance correction, taken during IS measurements using Ni/PGR as working electrode, Pt as counter electrode and Ag/AgCl as reference (RHE potential scale), in aqueous electrolytes containing 1 M LiOH and 0.5MLiOH/0.5 M LiCl with 0 mM and 40 mM HMF.

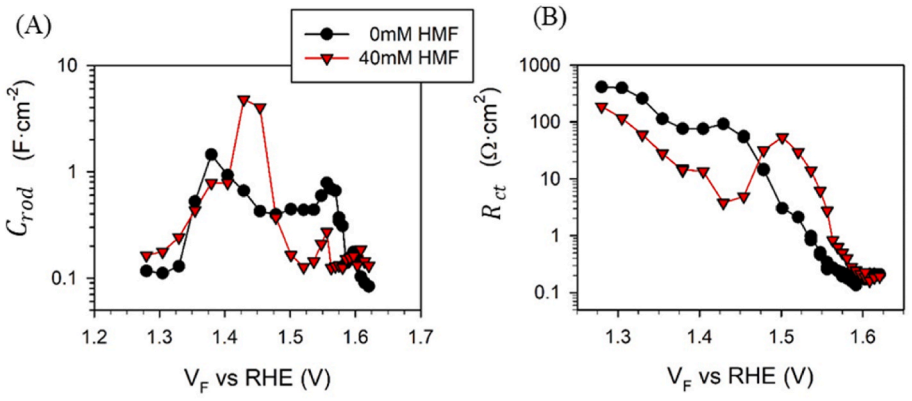

Fig. 6. Impedance analysis of samples without and with HMF in solution. A) C_{rod} and, B) R_{ct} for the fitting of IS measurements in 1 M LiOH.

for potential side reactions. This phenomenon could elucidate the challenges in detecting such intermediates using conventional techniques, as previously noted in the literature [25]. By using operando spectroscopic methods, some researchers have reported signals indicative of aldehyde adsorption on the Ni surface, notably lacking alcohol adsorption signals [27]. This explanation aligns with the possibility that species like HMFCA may indeed become adsorbed on the Ni electrodes, which agrees well with our IS experiments wherein a decrease in the C_{rod} was observed.

Further increase of the potential allowed to see again the C_{rod} peak associated to the onset of the OER, again at 1.55 V *vs* RHE. The related decrease in the R_{ct} values occurs after the oxidation of the intermediate species is completed. Then, the values of C_{rod} and R_{ct} resemble again to those from the HMF free solution.

The good match between the maximums of C_{rod} and the minimums for R_{ct}, confirms the relationship between the transition of the oxidation state and the charge transfer to the oxidized species, either if is the Ni^{2+}/Ni^{3+} redox couple, or the products obtained from HMF oxidation or OER.

4. Conclusions

HMF electro-oxidation to FDCA was reached with easily prepared Ni/PGR electrodes in basic media, obtaining FDCA as main product. Spontaneous degradation of HMF into formate has been minimized through the optimization of the electrolyte solution, by decreasing the amount of LiOH used. Under these reaction conditions, a 91 % FDCA yield was achieved after 6 h of reaction when employing a single Ni/PGR electrode. Remarkably, the reaction time could be significantly shortened to just 100 min, resulting in a 94 % yield, over 99 % conversion, and an 88 % Faraday efficiency when utilizing five Ni/PGR electrodes. These results are comparable to outcomes achieved with costlier and more intricate electrodes prepared through complex procedures. Impedance Spectroscopy allowed us to separate the different capacitance peaks associated to Ni^{2+}/Ni^{3+}, HMF oxidation and Ni^{3+}/Ni^{4+}. Furthermore, we have showcased the utility of Impedance analysis as an alternative method for identifying the adsorption of intermediate species on the electrode surface. In the context of HMF oxidation, this adsorption process facilitates subsequent reactions leading to the formation of FDCA. This insight helps elucidate why these intermediates remained elusive and undetectable during the reaction.

CRediT authorship contribution statement

David Carvajal: Investigation, Data curation, Formal analysis, Writing – original draft. **Ramón Arcas:** Investigation, Data curation,

Formal analysis. **Laxman Gouda:** Investigation. **Francisco Fabregat-Santiago:** Original idea, Methodology, Writing – review & editing, Resources, Funding acquisition. **Elena Mas-Marzá:** Original idea, Methodology, Writing – review & editing, Funding acquisition.

Declaration of competing interest

The authors declare that they have no known competing financial interests or personal relationships that could have appeared to influence the work reported in this paper.

Data availability

Data will be made available on request.

Acknowledgments

The authors want to acknowledge the projects ECOCAT ref. PID2020-116093RB-C41, funded by MCIN/AEI/10.13039/501100011033; UJI-B2022-33, funded by University Jaume I; and PROMETEO/2020/028, funded by Generalitat Valenciana. D.C. and L.G. acknowledge Generalitat Valenciana for grants GRISOLIAP/2019/057 and GRISOLIAP/2018/A/070, respectively. The authors thank Servicio Central de Instrumentación Científica (SCIC) from Universitat Jaume I for SEM and EDS measurements.

Appendix A. Supplementary data

Supplementary data to this article can be found online at https://doi.org/10.1016/j.matchemphys.2023.128510.

References

[1] J.L. Holechek, H.M.E. Geli, M.N. Sawalhah, R. Valdez, Sustainability 14 (2022) 4792.
[2] R. Xia, S. Overa, F. Jiao, JACS Au 2 (2022) 1054–1070.
[3] L.F.T. Novaes, J. Liu, Y. Shen, L. Lu, J.M. Meinhardt, S. Lin, Chem. Soc. Rev. 50 (2021) 7941–8002.
[4] W.-J. Liu, L. Dang, Z. Xu, H.-Q. Yu, S. Jin, G.W. Huber, ACS Catal. 8 (2018) 5533–5541.
[5] V. Kumaravel, J. Bartlett, S.C. Pillai, ACS Energy Lett. 5 (2020) 486–519.
[6] K. Sayama, ACS Energy Lett. 3 (2018) 1093–1101.
[7] N.-T. Suen, S.-F. Hung, Q. Quan, N. Zhang, Y.-J. Xu, H.M. Chen, Chem. Soc. Rev. 46 (2017) 337–365.
[8] C.R. Lhermitte, K. Sivula, ACS Catal. 9 (2019) 2007–2017.
[9] B. You, X. Liu, N. Jiang, Y. Sun, J. Am. Chem. Soc. 138 (2016) 13639–13646.
[10] Y. Yang, T. Mu, Green Chem. 23 (2021) 4228–4254.
[11] S. Chen, R. Wojcieszak, F. Dumeignil, E. Marceau, S. Royer, Chem. Rev. 118 (2018) 11023–11117.
[12] C. Chen, L. Wang, B. Zhu, Z. Zhou, S.I. El-Hout, J. Yang, J. Zhang, J. Energy Chem. 54 (2021) 528–554.
[13] M. Sajid, X. Zhao, D. Liu, Green Chem. 20 (2018) 5427–5453.
[14] Z. Zhang, K. Deng, ACS Catal. 5 (2015) 6529–6544.
[15] Y. Zhao, M. Cai, J. Xian, Y. Sun, G. Li, J. Mater. Chem. A 9 (2021) 20164–20183.
[16] B.J. Taitt, D.-H. Nam, K.-S. Choi, ACS Catal. 9 (2019) 660–670.
[17] Y. Yang, D. Xu, B. Zhang, Z. Xue, T. Mu, Chem. Eng. J. 433 (2022), 133842.
[18] D.A. Giannakoudakis, J.C. Colmenares, D. Tsiplakides, K.S. Triantafyllidis, ACS Sustain. Chem. Eng. 9 (2021) 1970–1993.
[19] G. Grabowski, J. Lewkowski, R. Skowroński, Electrochim. Acta 36 (1991) 1995.
[20] S. Barwe, J. Weidner, S. Cychy, D.M. Morales, S. Dieckhöfer, D. Hiltrop, J. Masa, M. Muhler, W. Schuhmann, Angew. Chem. Int. Ed. 57 (2018) 11460–11464.
[21] F.J. Holzhäuser, T. Janke, F. Öztas, C. Broicher, R. Palkovits, Advanced Sustainable Systems 4 (2020), 1900151.
[22] Z. Yang, B. Zhang, C. Yan, Z. Xue, T. Mu, Appl. Catal. B Environ. 330 (2023), 122590.
[23] H. Ait Rass, N. Essayem, M. Besson, ChemSusChem 8 (2015) 1206–1217.
[24] A. Danielli da Fonseca Ferreira, M. Dorneles de Mello, M.A.P. da Silva, Ind. Eng. Chem. Res. 58 (2019) 128–137.
[25] L. Gouda, L. Sévery, T. Moehl, E. Mas-Marzá, P. Adams, F. Fabregat-Santiago, S. D. Tilley, Green Chem. (2021), https://doi.org/10.1039/D1GC02031E.
[26] R. Arcas, Y. Koshino, E. Mas-Marzá, R. Tsuji, H. Masutani, E. Miura-Fujiwara, Y. Haruyama, S. Nakashima, S. Ito, F. Fabregat-Santiago, Sustain. Energy Fuels 5 (2021) 3929–3938.
[27] H. Zhou, Z. Li, L. Ma, H. Duan, Chem. Commun. 58 (2022) 897–907.
[28] V. Vedharathinam, G.G. Botte, Electrochim. Acta 108 (2013) 660–665.
[29] H. Noh, J.M. Mayer, Chem 8 (2022) 3324–3345.
[30] K. Gupta, R.K. Rai, A.D. Dwivedi, S.K. Singh, ChemCatChem 9 (2017) 2760–2767.
[31] H. Zhang, T. Gao, Q. Cao, W. Fang, ACS Sustain. Chem. Eng. 9 (2021) 6056–6067.
[32] X. Cheng, S. Li, S. Liu, Y. Xin, J. Yang, B. Chen, H. Liu, Chem. Commun. 58 (2022) 1183–1186.